

Design and Modeling of an Integrated Inductor in a Buck Converter DC-DC

Y. Benhadda^{1,*}, A. Hamid¹, T. Lebey², M. Derkaoui¹

¹ University of Sciences and Technology of Oran (USTO- MB) 31000 Algeria

² University of Paul Sabatier, LAPLACE Laboratory, Toulouse, France

(Received 20 March 2015; revised manuscript received 05 June 2015; published online 10 June 2015)

This paper presents the design and modeling of a square inductor for its integration in Buck converter DC-DC. The first, we calculate the value of inductance. The second, we describe our inductor; dimensioning and electrical model. A buck micro converter schematic simulation coupled with ideal and integrated inductor was presented. This conceptual model of the buck is best understood in terms of the relation between current and voltage of the inductor. Finally, we have simulated the electromagnetic effects in two cases. The first case, an inductor in the air, the second case with substrate. Our geometry is created in 3D space dimension.

Keywords: Inductor, Buck converter, Integrated.

PACS number: 84.32.Hh

1. INTRODUCTION

In Power electronics, modeling of passive components constitute a particularly important issue. Indeed, the magnetic components, inductors and transformers are mainly used to transmit or store energy. The passive elements volume reduction leads to a mounted in operating frequency, but this increase in frequency causes an increase in losses. If the behavior of some components is relatively insensitive to temperature changes, it is not the same thing for magnetic components whose characteristics depend strongly on the temperature. The losses freed in the form of heat are become a major concern due to the reduction of trade with the outside surfaces and increasing the density of losses. The aim of our work is a dimensioning a square inductor that will be integrated in a DC-DC micro-converter.

2. PRESENTATION OF THE MICRO-CONVERTER

We have chosen a Buck micro-converter continuous-continuous step-down (Fig.1) [1-3]. The inductor to integrate will thus be dimensioned for this type of application. Input voltage, $V_{in} = 3\text{ V}$. Output voltage, $V_{out} = 1.5\text{ V}$. Maximum current $I_{Lmax} = 0.65\text{ A}$. Output power, $P_{out} = 0.6\text{ W}$. Frequency of operation, $f = 1\text{ MHz}$.

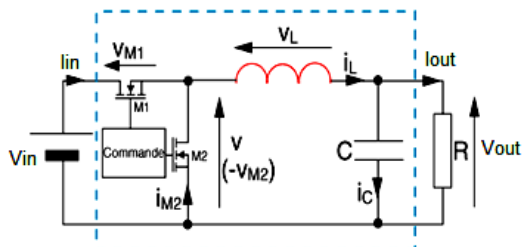


Fig. 1 – Buck converter

The converter operates in two modes of conduction discontinuous conduction when the current required by

the load is low, continuous conduction for higher currents (Fig. 2). The voltage and current involved are relatively low. In order to increase the efficiency of the converter, energy losses must be minimized.

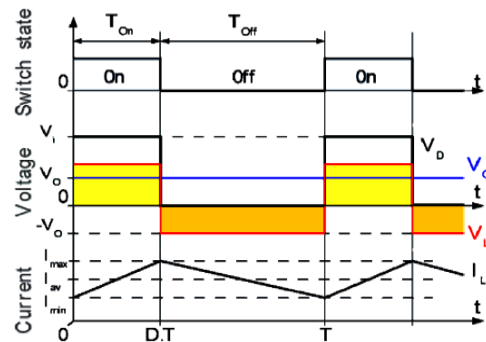


Fig. 2 – Evolution of the voltages and currents with time in an ideal buck converter

The average output current I_{out} is calculated by formula (1)

$$I_{out} = \frac{P_{out}}{V_{out}} \quad (1)$$

$I_{out} = 4\text{ A}$, $I_{out} = I_L - I_C$, $I_C = 0$, $I_{out} = I_L$. The peak amplitude of the current through the inductor is calculated by formula (2)

$$\Delta I_L = I_{Lmax} - I_{Lmin} \quad (2)$$

The average current I_L is expressed as follows (3)

$$I_L = \frac{I_{Lmax} + I_{Lmin}}{2} \quad (3)$$

Where

$$I_{Lmin} = 2I_{out} - I_{Lmax}, I_{Lmin} = 0.15\text{ A}, \Delta I_L = 0.5\text{ A} \text{ and } \alpha = V_{out}/V_{in} = 0.5.$$

* benhadda_yamina@yahoo.fr

The current which flows through the inductor increases according to relation (4)

$$\Delta I_L = \frac{\alpha(1-\alpha)V_{in}}{Lf} \quad (4)$$

We can calculate the value of the inductance L [2] according to relation (5)

$$L = \frac{\alpha(1-\alpha)V_{in}}{\Delta I_{if}} \quad (5)$$

The maximum energy stored in the inductor is given by relation (6)

$$W = \frac{1}{2}LI_{out}^2 \quad (6)$$

The volumetric energy density of the ferrite is given by the equation (7)

$$W_{vmax} = \frac{B_{max}^2}{2\mu_0\mu_r} \quad (7)$$

B_{max} : The maximum magnetic induction supported by the ferrite

μ_r : The relative permeability

μ_0 : The magnetic permeability of the free space

The volume of the ferrite is given by relation (8)

$$V_{ol} = \frac{W}{W_{vmax}} \quad (8)$$

The ferrite's thickness is $t_{sub} = 97 \mu\text{m}$, thus the volume will be $2100 \times 2100 \times 97 \mu\text{m}^3$.

3. DIMENSIONING OF THE INTEGRATED INDUCTOR

The geometry parameters characterizing the integrated inductor (Fig. 3) are the number of turns n , the width of the conductor w , thickness of the conductor t , the spacing between conductor s , length of the conductor l , the outer diameter d_{out} and input diameter d_{in} .

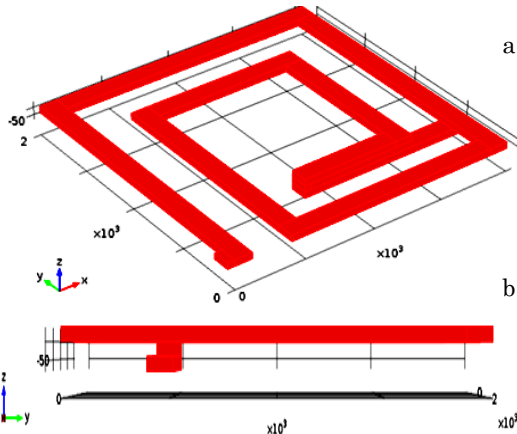


Fig. 3 – Geometry of a square spiral integrated inductor, (a) 3D view, (a) 2D view

We find in the literature several formulas which allow us to calculate the number of turns n according to the value of inductance L , we chose the Weeler's [4-5] formula (9)

$$L_{mw} = K_1\mu_0 \frac{n^2 d_{avg}}{1 + k_2\rho} \quad (9)$$

Where, we define the average diameter as $d_{avg} = (d_{out} + d_{in}) / 2$ [6]. A_m the factor's form defined as $A_m = d_{out} - d_{in} / d_{out} + d_{in}$. The coefficients k_1 and k_2 are defined for each geometry. For a square inductor spiral, $k_1 = 2.34$ and $k_2 = 2.75$.

The spacing between conductors is expressed as follows (10)

$$s = \frac{d_{out} + d_{in} - 2wn}{2(n-1)} \quad (10)$$

The length of the trace is expressed as follows (11)

$$l = 4n[d_{out} - (n-1)s - nw] - s \quad (11)$$

The skin thickness is defined as (12)

$$\delta = \sqrt{\frac{\rho}{\pi\mu f}}, \quad (12)$$

where ρ represent the resistivity of the conductor, $\rho_{Copper} = 1.7 \cdot 10^{-8} \Omega\text{m}$ and μ its magnetic permeability.

So that the current flows in the entire conductor, it is necessary that one of the following conditions is filled, $w \leq 2\delta$ or $t \leq 2\delta$, $\delta = 92.8 \mu\text{m}$, $t = 40 \mu\text{m}$, $w = 120 \mu\text{m}$. Table 1 contains the specifications and the design results of the square spiral integrated inductor.

Table 1 – Design results of the square spiral integrated inductor

Parameter	Value
Inductance, L (μH)	1.5
External diameter, d_{out} (mm)	2
Internal diameter, d_{in} (mm)	0.4
Number of turns, n	2
Thickness of the conductor, t (μm)	40
Width of the conductor, w (μm)	120
Spacing between conductor, s (μm)	280
Length of the conductor, l (m)	0.0116

4. ELECTRICAL MODEL

The equivalent electrical model of the integrated inductor [6-10] [15-16] is shown in Fig. 4.

The series resistance R_s , can be approximated as (13)

$$R_s = \rho l / wt \quad (13)$$

The parasitic capacitive can be modeled as C_s (14)

$$C_s = t\varepsilon_0 l^2 / s \quad (14)$$

where, ε_0 is the permittivity of free space, $\varepsilon_0 = 8.854187 \cdot 10^{-12} \text{Mm}^{-1}$.

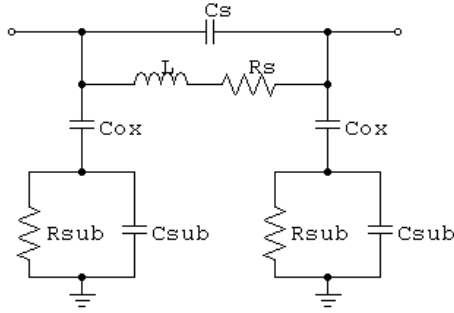


Fig. 4 – Equivalent electrical model

The substrate capacitance C_{sub} and resistance R_{sub} are approximately proportional to the area occupied by the integrated inductor and can be expressed as (15), (16).

$$C_{sub} = \frac{1}{2} \epsilon_0 \epsilon_r \frac{lw}{t_{sub}} \quad (15)$$

$$R_{sub} = 2\rho_{sub} \frac{t_{sub}}{lw} \quad (16)$$

C_{ox} oxide capacitance SiO_2 can be expressed as (17)

$$C_{ox} = lw \left(\frac{\epsilon_0 \epsilon_{ox}}{t_{ox}} \right), \quad (17)$$

where ϵ_r, ρ_{sub} represent respectively the relative permittivity and the resistivity of substrate and t_{ox} the oxide thickness. In our case, $\epsilon_r = 10$, $\rho_{sub} = 45.10^{-6} \Omega m$ and $t_{ox} = 80 \mu m$.

The geometry of a square spiral integrated inductor on substrate [13-14] is shown in Fig. 5.

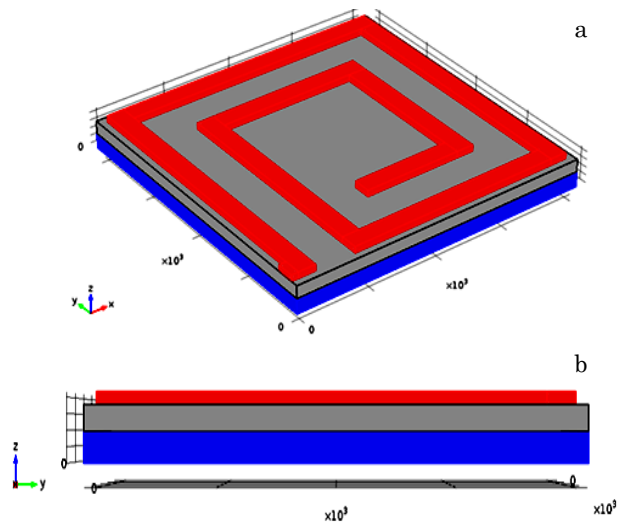


Fig. 5 – Geometry of a square spiral integrated inductor on substrate, (a) 3D view, (b) 2D view

The efficiency of integrated inductor is calculated [16-20] according by relation (18)

$$Q = 2\pi \frac{\text{stocked energie}}{\text{dissipated energie}} \quad (18)$$

Table 2 presents electrical parameters of the integrated inductor.

Table 2 – Electricals Parameters of the Integrated Inductor

Electricals parameters	Values
$R_s(\Omega)$	0.04
$R_{sub}(\Omega)$	0.006
$C_s(pF)$	0.014
$C_{ox}(pF)$	0.598
$C_{sub}(pF)$	0.631
Q	98.56

Fig. 6 shows the shape of the quality factor as a function of frequency.

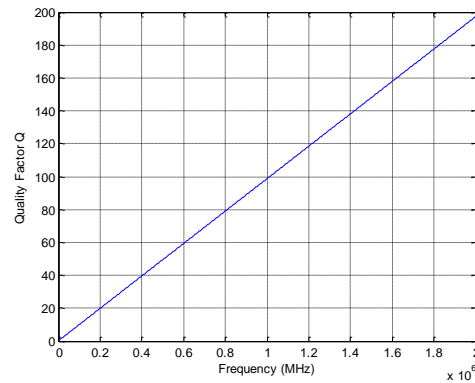


Fig. 6 – Quality factor Q from integrated inductor

5. SIMULATION OF THE OF THE MICRO CONVERTER

In this simulation, the circuit of Fig. 7 contains an ideal inductor and the Fig. 8 shows the waveform of the output voltage and current of the Buck micro converter. When the switch is closed, the voltage across the inductor is $V_L = V_{in} - V_{out}$. The current through the inductor rises linearly. As the diode is reverse-biased by the voltage source, no current flows through it. When the switch is opened, the diode is forward biased. The voltage across the inductor is $V_L = -V_{out}$. The Current through inductor decreases.

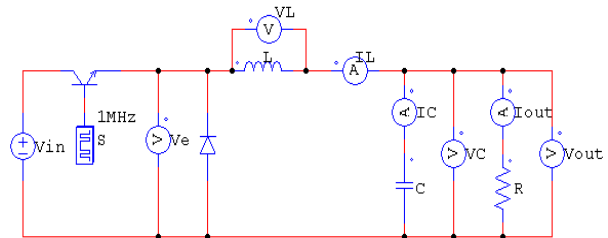


Fig. 7 – Schematic of buck micro converter coupled with ideal inductor

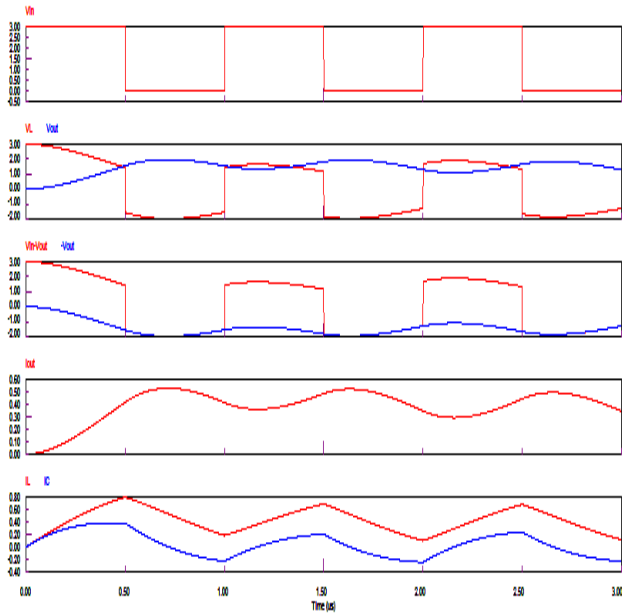


Fig. 8 – Waveforms of voltage and current of buck micro converter coupled with ideal inductor

Fig. 9 shows the schematic of micro converter simulated coupled with integrated inductor. The simulated results are indicated in Fig. 10. We observe the same result with ideal inductor.

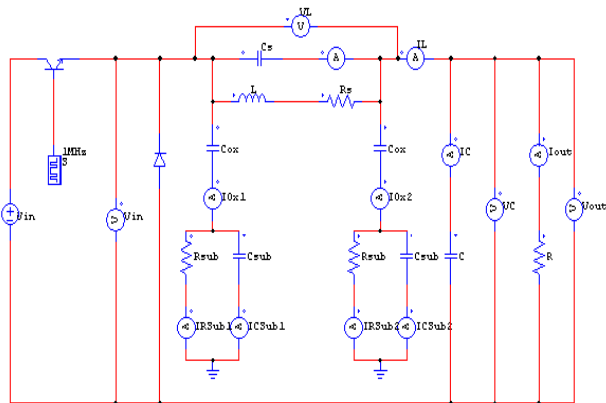


Fig. 9 – Schematic of buck micro converter coupled with integrated inductor

6. SIMULATION 3D OF THE ELECTROMAGNETIC EFFECTS IN A INTEGRATED INDUCTOR

In this section, we present the distribution of the electromagnetic field in a inductor in the air and on substrate [21] using finite elements method [22-24].

Fig. 11 shows the distribution of magnetic field in the inductor in the air.

Fig. 12 shows the distribution of magnetic field lines in the inductor in the air.

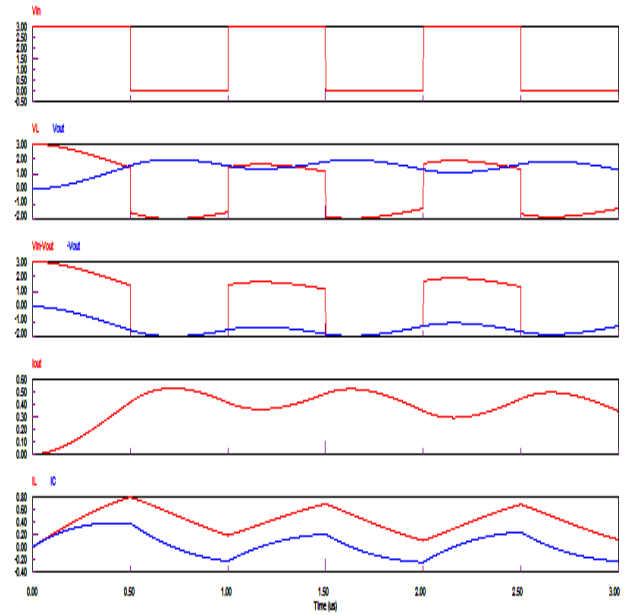


Fig. 10 – Waveforms of voltage and current of buck micro converter coupled with integrated inductor

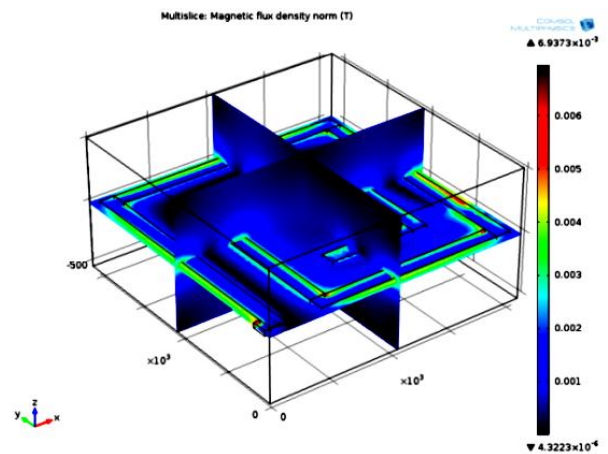
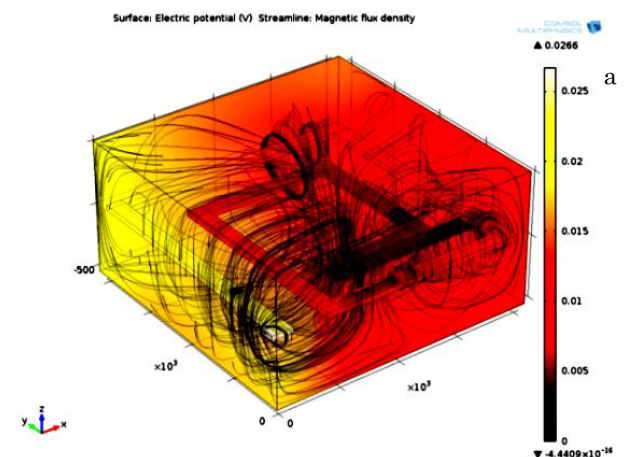


Fig. 11 – Distribution of magnetic field in the inductor in the air



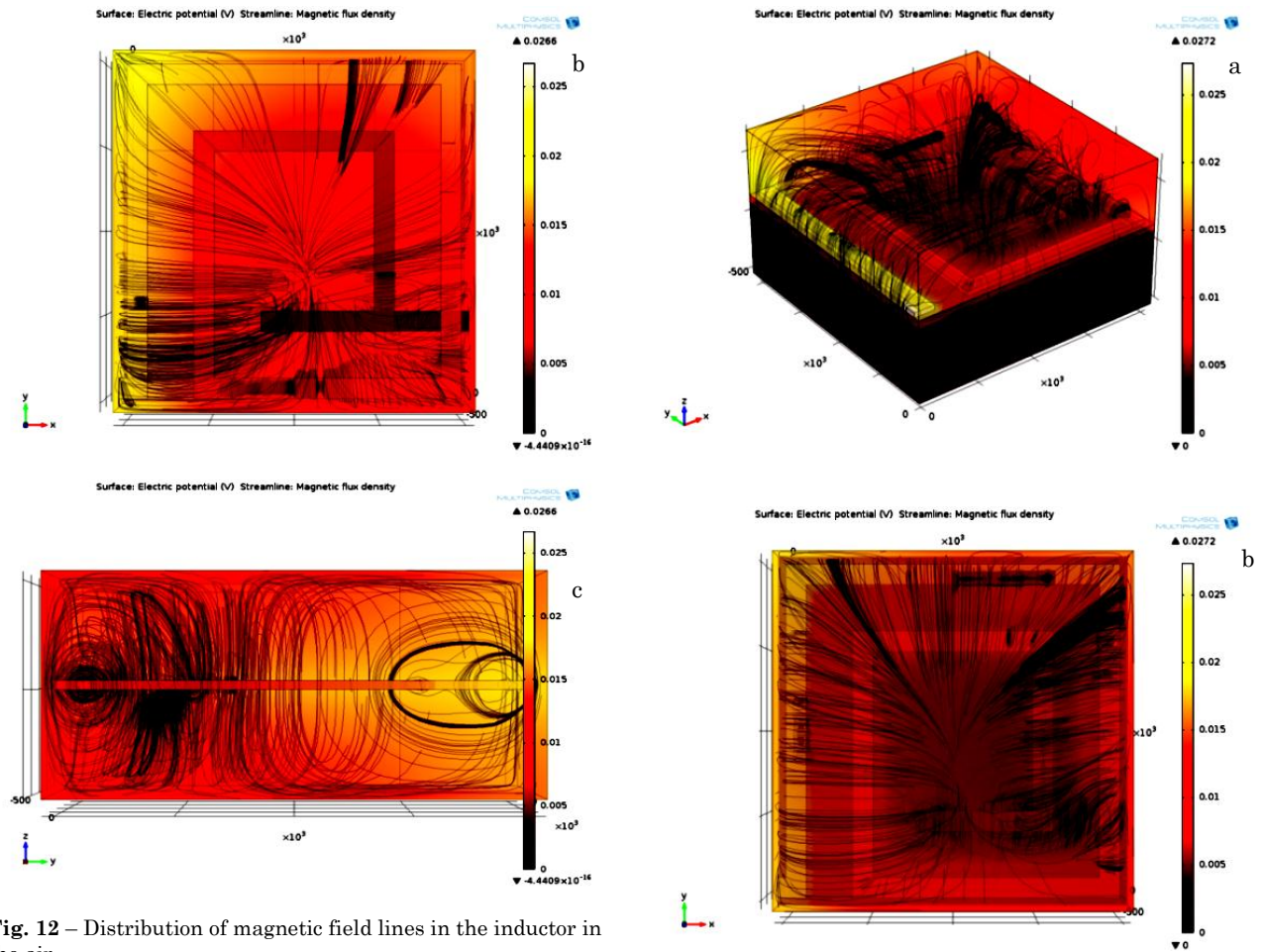


Fig. 12 – Distribution of magnetic field lines in the inductor in the air

Fig. 13 shows the distribution of magnetic field in the inductor on substrate.

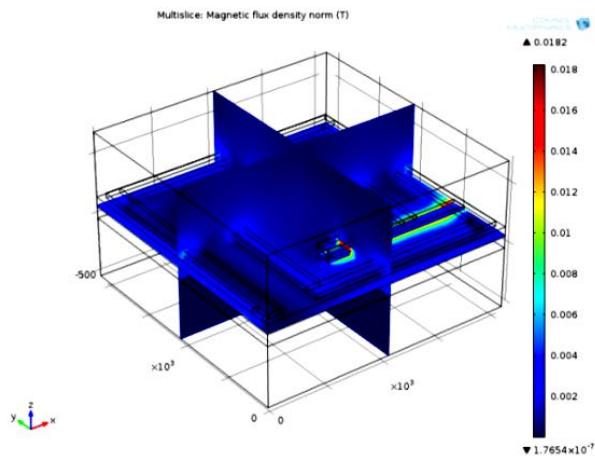


Fig. 13 – Distribution of magnetic field in the inductor on substrate

Fig. 14 shows the distribution of magnetic field lines in the inductor on substrate. When we insert a substrate, the majority of the magnetic field lines are concentrated at the walls of the magnetic block. So, we conclude that the substrate layer is required to have a good electromagnetic compatibility in the case of the integration inductor.

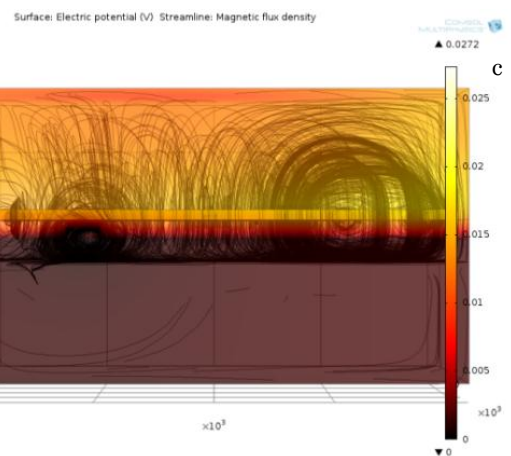


Fig. 14 – Distribution of magnetic field lines in the inductor on substrate

7. CONCLUSION

In this paper, we have presented the dimensioning, the modeling and the simulation of a square inductor. We have visualized the electromagnetic phenomenon in inductor in the air and on substrate. The aim of this simulation is to study the electromagnetic compatibility of the inductor integrated in Buck micro converter DC-DC.

REFERENCES

1. P. Reimann, *Phys. Rep.* **361**, 57 (2002).
2. G.S. Vorobjov, V.O. Zhurba, A.S. Krivets, *J. Nano-Electron. Phys.* **2** No 4, 47 (2010).
3. L. Xian, Y. Wang An, *11th IEEE Int. Conf. Control Automation (ICCA)* 1067 (2014).
4. A. Allaoui, A. Hamid, P. Spiterri, V. Bley, T. Lebey, *J. Low Power Electron.* **11** No 1, 63 (2015).
5. M. Derkaoui, A. Hamid, T. Lebey, R. Melati, *Telkomnika* **11** No 4 (2013).
6. S.S. Mohan, M.D.M. Hershenson, S.P. Boyd, T.H. Lee, *IEEE J. Solid-State Circuits* **34** No 10, 1419 (1999).
7. N. Arbabi, M. Najmabadi, V. Devabhaktuni, M. Yagoub, *Canadian Conf. Electrical Computer Eng. (CCECE)*, 99 (Vancouver, BC: Canada: 2007).
8. E.D. Gadjeva, V.P. Durev, M.H. Hristov, D.I. Pukneva, *Proc. of the 13th Int. Conf. Mixed Design of Integrated Circuits and Systems MIXDES*, 518 (Gdynia: Poland: 2006).
9. R. Guo, C. Wang, T. Li, *8th IEEE Conference on Industrial Electronics and Applications (ICIEA 2013)* (2013).
10. C.P. Yue, C. Ryu, J. Lau, T.H. Lee, S.S. Wong, *IEEE Electron Dev. Meeting*, 155 (1996).
11. H. Fuketa, Shinozuka, K. Ishida, M. Takamiya, T. Sakurai, *IEEE Power Electron. Conf.*, 2228 (2014).
12. M. Kaluza, A. Napieralski, *Bulletin of the Polish Academy of Sciences Technical Sciences* **56** No 1, 21 (2008).
13. A. Tasic W.A. Serdijn, *IEEE Int. Symp. on Circuits and Systems, II-819* (2002).
14. C.P. Yue, S.S. Wong, *IEEE T. Electron Dev.* **47** No 3, 560 (2000).
15. M.K. Yapici, J.M. Hong, J. Zou, K. Balareddy, *IEEE 17th Int. Conf. Transducers and Eurosensors XXVII*, 128 (2013).
16. C.-H. Liu, H.-D. Chang, K.-H. Li, C.H. Lin, C.-J. Hsu, T.-Y. Lin, H.-H. Chou, H.-C. Huang, H.-Y. Liao, *IEEE Electron. Components Technol. Conf.* 1675 (2013).
17. C.P. Yue, S.S. Wong, *IEEE J. Solid-State Circuits* **33** No 5, 743 (1998).
18. T.G. Imre, U. Viscarret, I.E. Otadui, A. Rufer, *IEEE* (2008).
19. C. Wang, H. Liao, C. Li, R. Huang, W. Wong, X. Zhang, Y. Wang, *IEEE T. Electron Dev.* **56** No 4, 609 (2009).
20. S.Y. Lee, L. Zhao, J.T. Strydom, W.G. Odendaal, J.D. Van Wyk, *IEEE 33rd Annual Power Electronics Specialists Conf.*, 1009 (2002).
21. R. Petkov, *IEEE T. Power Electron.* **11** No 1, 33 (1996).
22. P. Viarouge, J.C. Fagundes, E. Tourkhani, H. Le-Huy, *IEEE Canadian Conference on Electrical and Computer Engineering*, 582 (1995).
23. P. Sharma, M. Mehta, *Int. J. Sci. Eng. Res.* **3** No 2, (2012).
24. Q. Qian, Y. Liu, *IEEE* (2013).
25. M.-C. Hsieh, *IEEE T. Components, Packaging Manufacturing Technol.* **4** No 3, 451 (2014).
26. L. Ying, H. Chunyue, Z. Xin, L. Tianming, G. Guangkuo, X. Guoji, T. Wenliang, *IEEE 15th Int. Conf. Electronic Packaging Technol. (ICEPT)*, 577 (2014).